JACS
JOURNAL OF THE AMERICAN CHEMICAL SOCIETY
Article
pubs.acs.org/JACS

Reactivity of the Excited States of the H-Cluster of FeFe Hydrogenases

Matteo Sensi,[†,▽] Carole Baffert,[†] Claudio Greco,[‡] Giorgio Caserta,[§] Charles Gauquelin,[∥] Laure Saujet,[⊥] Marc Fontecave,[§] Souvik Roy,[#] Vincent Artero,[#] Philippe Soucaille,[∥] Isabelle Meynial-Salles,[∥] Hervé Bottin,[⊥] Luca de Gioia,[▽] Vincent Fourmond,[†] Christophe Léger,[*,†] and Luca Bertini[*,▽]

[†]Aix Marseille Univ., CNRS, BIP UMR 7281, Marseille, France

[‡]Department of Earth and Environmental Sciences, Milano-Bicocca University, Piazza della Scienza 1, 20126 Milan, Italy

[§]Laboratoire de Chimie des Processus Biologiques, UMR 8229 CNRS, Collège de France, Université Paris 6, 11 Place Marcelin Berthelot, Paris 75231 Cedex 05, France

[∥]Université de Toulouse, INSA, UPS, INP, LISBP, INRA:UMR792,135 CNRS:UMR 5504, avenue de Rangueil, 31077 Toulouse, France

[⊥]Institut de Biologie et de Technologies de Saclay IBITECS, SB2SM/Institut de Biologie Intégrative de la Cellule I2BC, UMR 9198, CEA, CNRS, Université Paris Sud, F-91191 Gif sur Yvette, France

[#]Laboratoire de Chimie et Biologie des Métaux, Université Grenoble Alpes, CNRS, CEA, 17 rue des Martyrs, 38054 Grenoble, France

[▽]Department of Biotechnologies and Biosciences, University of Milano-Bicocca, Piazza della Scienza 2, 20126 Milan, Italy

Supporting Information

ABSTRACT: FeFe hydrogenases catalyze H_2 oxidation and formation at an inorganic active site (the "H-cluster"), which consists of a $[Fe_2(CO)_3(CN)_2$(dithiomethylamine)] subcluster covalently attached to a Fe_4S_4 subcluster. This active site is photosensitive: visible light has been shown to induce the release of exogenous CO (a reversible inhibitor of the enzyme), shuffle the intrinsic CO ligands, and even destroy the H-cluster. These reactions must be understood because they may negatively impact the use of hydrogenase for the photoproduction of H_2. Here, we explore in great detail the reactivity of the excited states of the H-cluster under catalytic conditions by examining, both experimentally and using TDDFT calculations, the simplest photochemical reaction: the binding and release of exogenous CO. A simple dyad model can be used to predict which excitations are active. This strategy could be used for probing other aspects of the photoreactivity of the H-cluster.

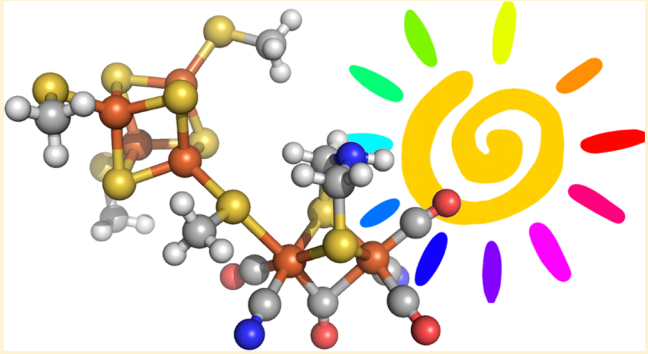

INTRODUCTION

Hydrogenases are metalloenzymes that oxidize and produce dihydrogen.[1−3] They are involved in the bioenergetic metabolism of most microorganisms. The observation that light reverses the inhibition by CO of certain hydrogenases was made soon after these enzymes were first identified in the 1930s; the photosensitivity of the CO-bound complex and the competitive character of the inhibition were used to demonstrate that both exogenous CO and substrate H_2 bind to an active site iron atom.[4] Now we know that there are two types of hydrogenase active sites, and that the photorelease of CO under catalytic conditions was only observed with the so-called "FeFe hydrogenases" (see however ref 5 for a report of CO photorelease from NiFe hydrogenase under cryogenic conditions).

The active site of FeFe hydrogenase is a $[Fe_2(CO)_3(CN)_2$-(dithiomethylamine)] subcluster covalently attached to a Fe_4S_4 subcluster, as depicted in Figure 1A.[6−9] The 2Fe subcluster bears terminal and bridging intrinsic CO and CN^- ligands. The

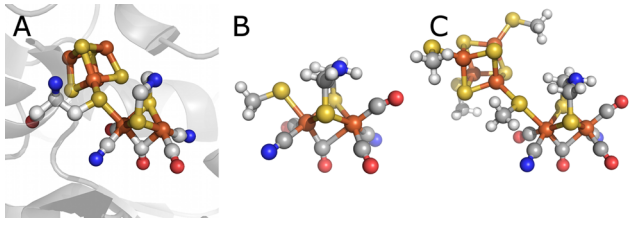

Figure 1. H-cluster of hydrogenase. (A) Structures of the active site of *C. acetobutylicum* FeFe hydrogenase, adapted from pdb 3C8Y.[23] (B and C) Two models of H_{ox}−CO used in our TDDFT calculations.

Received: June 30, 2016
Published: September 20, 2016

DOI: 10.1021/jacs.6b06603
J. Am. Chem. Soc. 2016, 138, 13612−13618

binding of exogenous CO to the "distal" Fe (outermost, Fe_d) of the active site in the H_{ox} redox state ($Fe^{I}Fe^{II}$) yields the inhibited H_{ox}–CO form of the enzyme.[10] Exogenous CO dissociates to give back the active form of the H-cluster upon irradiation with white light either at room temperature[4,11] or at cryogenic temperature below 20 K, but other photoproducts are formed upon irradiation at cryogenic temperature in the range 20–80 K.[12−15] Albracht, Stripp, and co-workers have also shown that the CO ligands that are bridging and terminally bound on Fe_d can be exchanged with extrinsic CO upon illumination;[14−16] this shuffling of the coordination sphere of Fe_d is relevant to the reversible inactivation of the enzyme that occurs in the dark under oxidizing conditions.[17] The photosensitivity of the iron–carbonyl bonds can also lead to photoinduced damage when the enzyme is illuminated in the absence of exogenous CO; indeed, according to a study of the hydrogenase from *D. desulfuricans*,[14,15] long exposure to "normal laboratory light" at room temperature destroys the H-cluster. Such photodamage adds biotechnological barriers that will limit the effectiveness of H_2-photoproduction processes, whether they consist of using FeFe hydrogenases attached to photosensitizers[18,19] or microorganisms that couple photosynthesis to hydrogen production.[20] NiFe hydrogenases, in contrast, are apparently not damaged by light.[21,22]

The photolability of CO is a typical aspect of the reactivity of all transition metal carbonyl complexes, which has been investigated in dinuclear models of the H-cluster.[24] UV irradiation triggers CO photolysis in model compounds such as μ-propanedithiolate-$Fe_2(CO)_6$ and its derivatives; this has been studied using ultrafast transient IR spectroscopy,[25,26] and is supported by Density Functional Theory (DFT) calculations.[27] This reactivity is very solvent and ligand-dependent, and more complex than in the enzyme, probably because the protein that surrounds the active site prevents certain transformations. Time-dependent DFT (TDDFT) simulations shed light on the early stages of the photodynamics, showing that CO is loosely bound on the low energy excited-state surfaces, and that the photoreactivity strongly depends on the coordination sphere of the iron atoms.[28]

Here, we examine in great detail, both experimentally and theoretically, the effect of visible irradiation on the simplest reaction of the H-cluster: binding and release of the extrinsic inhibitor CO. We compare the results obtained with three different FeFe hydrogenases, and we examine for the first time how wavelength and light power affect the kinetics of inhibition under turnover conditions. The results are explained by TDDFT calculations of the electronic spectra and excited-state PES topologies of two different H_{ox}–CO models, which show how the photodynamics of the system depends on the nature and excitation energy of the electronic transitions considered. A very simple description of the system in terms of a donor–acceptor molecular dyad system proves useful for identifying which excitations contribute to CO photolysis, although we conclude that intramolecular charge transfer is not the main photochemical process resulting in CO release.

RESULTS/ELECTROCHEMISTRY

We have previously described a method for measuring the rates of CO binding and release to/from hydrogenases.[29,30] Briefly, a tiny amount of purified enzyme is either adsorbed or covalently attached[31] to a rotating disc electrode and inserted into the H_2-saturated solution of an electrochemical cell. Catalytic H_2 oxidation results in a positive current whose magnitude is proportional to turnover rate. The enzyme is repeatedly exposed to CO by injecting a small amount of CO-saturated buffer in the electrochemical cell; the concentration of inhibitor instantly increases and then decays because CO is constantly flushed away from the cell by the flow of H_2; the decay is exponential,[32,33] as indicated in Figure 2A, with time constant τ.

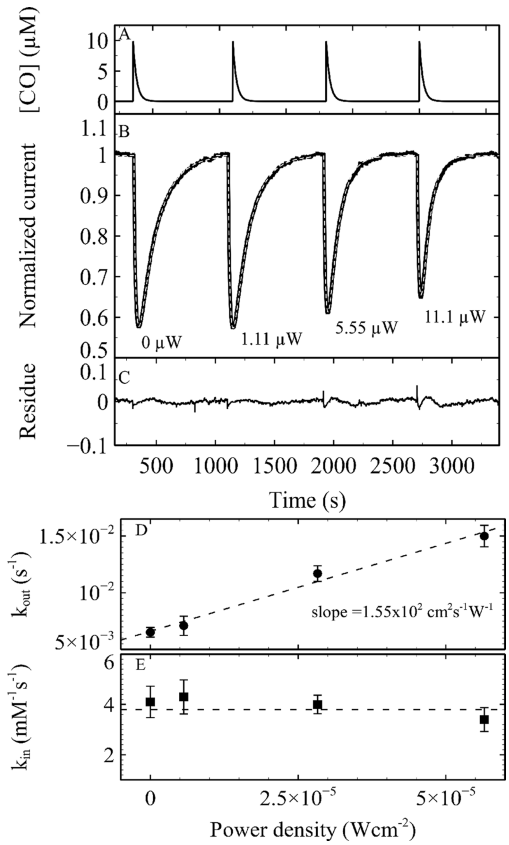

Figure 2. Electrochemical experiment showing the effect of 450 nm irradiation on the inhibition by CO of the FeFe hydrogenase from *M. elsdenii*. Data obtained with the FeFe hydrogenases from *C. acetobutylicum* and *C. reinhardtii* are shown in Supporting Information section 3.1, Supplementary Figures 18 and 19. Panel A shows the change in CO concentration against time, and panel B shows the resulting change in turnover rate and the fit of the kinetic model (dotted line), adjusting four values of k_{in}, four values of k_{out}, and a single value of τ. Panel C shows the residue of the fit. The fit returned the values of the rate constants shown in panels D and E. The *Y*-errors show the standard deviations observed in two independent experiments (the error on k_{in} includes the error in the value of $[CO]_0$). $p(H_2)$ = 1 atm, $[CO]_0$ = 10 μM, τ = 18 s, pH = 7, T = 30 °C. Electrode rotation rate = 3000 rpm.

The resulting change in catalytic current (turnover rate) is illustrated in Figure 2B. The current decreases after each injection at a rate that depends on the second-order rate constant of CO binding to the enzyme (k_{in}), and returns to its initial value after the CO concentration goes back to zero, at a rate that depends on the first-order rate constant of CO release (k_{out}) and on the value of τ. The change in current can be analyzed to measure k_{in}, k_{out}, and τ (when experiments such as that in Figure 2 are analyzed, the value of τ is forced to be the same in the fitting procedure for all four injections).

Here, we describe how the irradiation of the enzyme changes the kinetics of binding and release of CO under turnover conditions. The experimental setup that we used in this

DOI: 10.1021/jacs.6b06603
J. Am. Chem. Soc. 2016, 138, 13612−13618

investigation is such that the parallel beam of a monochromatic laser diode (λ = 405, 450, 532, or 635 nm) is directed upward, toward the electrode surface, across a quartz window at the bottom of the thermostated electrochemical cell. The experiment in Figure 2 was performed by adding the same amount of CO four times in a row, the first time in the dark (actually, with the low intensity of the light of the lab), and then after increasing stepwise the power output of the diode, *P*, as indicated.

Figure 2B shows that all things being equal, the more powerful is the 450 nm light, the less pronounced is the inhibition. The effect is small, but it is revealed by the fit of the model (dotted line), which allows the values of k_{in} and k_{out} to be precisely measured. Figure 2D shows that illumination with violet/blue light (405 or 450 nm) has a significant effect on k_{out} (up to 3-fold at maximal power) and none on k_{in}. Green or red light (532 or 635 nm) has an effect neither on CO binding nor on CO release. We show in Figure 3 the slope of the linear

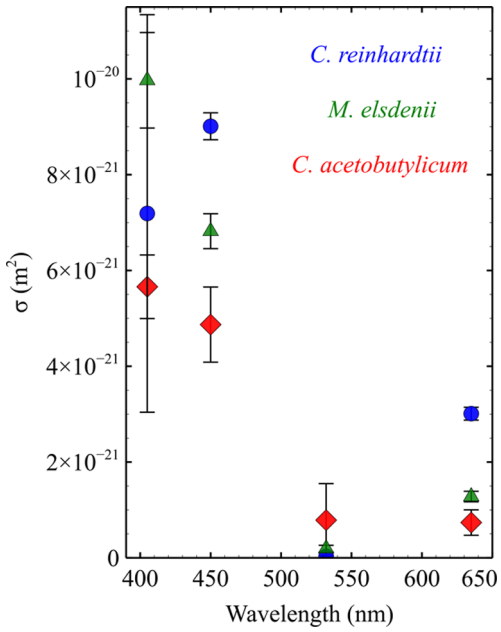

Figure 3. Dependence on wavelength of the effective cross section for the photodissociation of CO (calculated from the slope of the line in Figure 2D multiplied by $h\nu$) on the rate of CO release from the active site of the FeFe hydrogenases from *C. reinhardtii* (blue), *C. acetobutylicum* (red), and *M. elsdenii* (green).

change in k_{out} as a function of wavelength (expressed as a cross section) against power density, for experiments carried out with three distinct FeFe hydrogenases: those from *C. reinhardtii*,[34] *M. elsdenii*,[35] and *C. acetobutylicum*.[23] The enzyme from *C. reinhardtii* has no other cofactor than the H-cluster, whereas the other two bear additional electron-transferring FeS clusters.[1,23,34,35] In all cases, only violet/blue light (λ < 500 nm) has a detectable effect on k_{out}. The effect is about the same for all three enzymes (although its magnitude decreases in the order *M. eldensii* > *C. reinhardtii* > *C. acetobutylicum*, for reasons that cannot be elucidated at that point). Therefore, our experiments reveal an intrinsic property of the conserved H-cluster.

The change in kinetics of inhibition is not an artifact from heating. Indeed, in control experiments, we observed a current variation of less than 5 nA (<0.5% of the value of the current) when the laser diode (any wavelength) was suddenly switched on at maximal power, whereas the catalytic current increases 2-fold upon increasing the temperature from 10 to 35 °C, showing that the light-induced temperature variation is lower than 0.1 °C. For *Clostridium acetobutylicum*, we measured an activation energy for CO release in the dark of 74 kJ/mol (in the range 16−32 °C, Supplementary Figure 20); therefore, a temperature variation of 0.1 °C increases the rate of CO release no more than 1%. Incidentally, we note that this value of the activation energy is very close to the value that we calculate in Supporting Information section 2.3 (Supplementary Table 7) and Figure 4A with the small model of the active site.

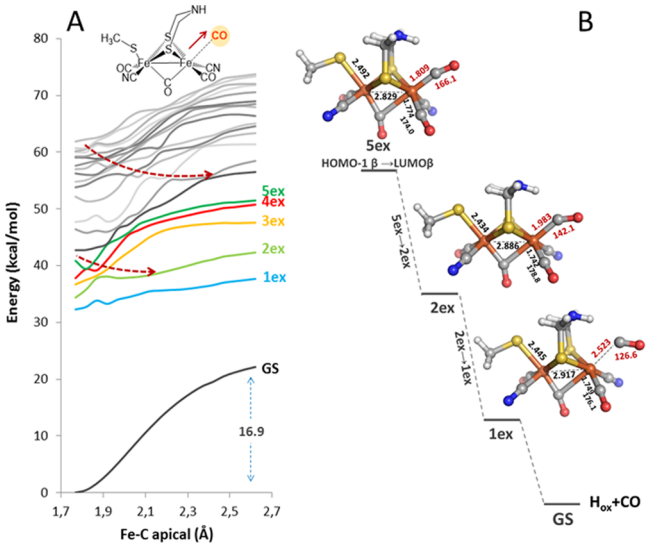

Figure 4. (A) Potential energy surfaces of the ground state and the first 20 excited doublet states of Fe_2S_2 H_{ox}−CO model along the apical Fe−C stretching coordinate. Energy differences in kcal/mol, computed with respect to the minimum ground-state energy. The value of the free energy dissociation barrier is also reported, and compares well with the experimental value determined in experiments shown in Supplementary Figure 20. Red arrows guide the eye to follow the dissociation pathway through the surface crossings. (B) Geometry-optimized structures for the Fe_2S_2 fifth (5ex) excited state, along the CO dissociation pathway. Distances in angstroms, angles in degrees.

TDDFT MODELING

We use previously described methods[36−38] to characterize the electronic structure of the CO-inhibited H-cluster on the basis of the composition and energy diagram of their molecular orbital (MO) (Supplementary Figure 3a,b). Each MO can be labeled according to its localization on the Fe_4S_4 or Fe_2S_2 fragment. This classification will help the discussion of the electronic transitions of the H-cluster, which we shall consider as a dyad system, consisting of a Fe_4S_4 cubane covalently linked to the Fe_2S_2 subcluster.

Scheme 1 depicts the four possible types of electronic transitions in the H-cluster. The fragment localized excitations are those in which the monoelectronic transitions involve MO localized on a single fragment (Fe_4S_4 or Fe_2S_2), while charge-transfer (CT) excitations involve MO localized on different fragments, yielding $Fe_4S_4 \rightarrow Fe_2S_2$ or $Fe_2S_2 \rightarrow Fe_4S_4$ CT states, which might decay toward their corresponding CT species.

We shall use Scheme 1 to discuss the excitations of the CO inhibited H-cluster based on their propensity to induce CO

DOI: 10.1021/jacs.6b06603
J. Am. Chem. Soc. 2016, 138, 13612−13618

Scheme 1. H-Cluster Electronic Excitation Resulting from Frontier MO Composition

Fragment localized states	Charge-transfer states
$[Fe_4S_4]^*$ — $[Fe_2S_2]$	$[Fe_4S_4]^{\delta+}$ — $[Fe_2S_2]^{\delta-}$
$[Fe_4S_4]$ — $[Fe_2S_2]^*$	$[Fe_4S_4]^{\delta-}$ — $[Fe_2S_2]^{\delta+}$

[a]From left: fragment localized (in red) states (on Fe_4S_4 or Fe_2S_2), and $Fe_4S_4 \rightarrow Fe_2S_2/Fe_2S_2 \rightarrow Fe_4S_4$ charge-transfer states.

release, which should increase in the order Fe_4S_4-localized < $Fe_2S_2 \rightarrow Fe_4S_4$ CT states < $Fe_4S_4 \rightarrow Fe_2S_2$ CT states < Fe_2S_2 localized. Indeed, the Fe_4S_4 localized states are inactive with respect to CO photolysis because the MOs involved do not show any Fe−CO orbital contributions (Supporting Information section 2.1). The $Fe_2S_2 \rightarrow Fe_4S_4$ CT states can decay via transient $Fe_4S_4^-$−$Fe_2S_2^+$ species, which should bind CO even more strongly than the H_{ox}−CO ground state because the Fe(II)Fe(II)CO fragment is undersaturated. In contrast, the decay of the $Fe_4S_4 \rightarrow Fe_2S_2$ CT states states toward $Fe_4S_4^+$−$Fe_2S_2^-$ species should result in the formation of a transient Fe(I)Fe(I)CO fragment, characterized by lower affinity for CO and lower dissociation barriers.[27,36] In the case of the CT states, the Fe−C bonding MO remains singly occupied, and the corresponding potential energy surface (PES) cannot be fully dissociative. The Fe_2S_2 localized states should be the most active toward CO photolysis because an Fe−C antibonding/nonbonding MO is populated to the detriment of a Fe−C bonding MO, as observed previously in studies of biomimetic models of the H-cluster.[27,39,40]

To confirm the above model, we computed the electronic spectrum of the full Fe_6S_6 H_{ox}−CO system (Figure 1C) and a structural model of the CO-bound Fe_2S_2 fragment (Figure 1B), the latter either including or excluding the side chains or the residues that form the H-bond network around the dtma and cyanide ligands (Supplementary Figure 11). The relationship between computed excitation energies and experimental wavelength irradiation is proposed in Supporting Information section 2.5, on the basis of the comparison of TDDFT spectra computed for different models (adopting pure GGA BP86 and the hybrid PBE0 functionals) and the UV−vis spectrum of the noninhibited enzyme.[41] We must emphasize that the computed excitation energies for the Fe_6S_6 model are not reliable enough for quantitative comparison with the experimental spectrum due to the highly negative total charge of the model, but the nature of the excitations and main mono electronic transitions can be compared to those calculated with the smaller model, for example, to identify the Fe_2S_2 localized excitations. Indeed, the comparison between BP86 and PBE0 shows the well-known blue shift of the excitation energy, but not significant change in the nature of the excited states (Supplementary Figure 12a).

Considering the Fe_6S_6 model, we computed the first BP86 600 excitations, and we observed that most of them are of the Fe_4S_4 localized type (they involve a large number of Fe_4S_4 localized MOs, and the excitations are described as Fe → S or S → Fe intracubane CT states) (Supplementary Table 2). In the low energy part of the spectrum, several weak $Fe_4S_4 \rightarrow Fe_2S_2$ CT excitations involve the Fe_2S_2 localized LUMOβ, while the intense band at higher energy results from the superposition of a large number of excitations including Fe_2S_2 localized transitions. In the middle of the spectrum, we identify three moderately intense excitations (two Fe_4S_4 localized and one $Fe_4S_4 \rightarrow Fe_2S_2$ CT) that should correspond to the shoulder at 415 nm in the experimental spectrum.[41] We conclude that higher energy irradiation is more effective with respect to CO photolysis because it populates Fe_2S_2 localized states, whereas lower energy irradiation populates $Fe_4S_4 \rightarrow Fe_2S_2$ CT states that are not fully dissociative.

This investigation of the Fe_6S_6 model fully supports the "pencil and paper" donor−acceptor model, by confirming the fragment localized and CT nature of the excitations as proposed in Scheme 1. To reach more definite conclusions, we had to explore the excited-state surfaces of the Fe_2S_2 model, as described below (unfortunately, we could not investigate the excited PES topology of the relevant states for the large model).

The computed electronic spectrum of the small model (Figure 1B) is dominated by ligand to metal and metal to ligand charge-transfer (LMCT and MLCT) excitations (Supplementary Tables 5 and 6). To identify the Fe-CO loosely bound excited states, a first approach is to explore the excited PES along the CO dissociation pathways on the ground-state PES. Considering the first 20 doublet excitations (hereafter referred to as "*n*ex", with n = 1−20), we observed a different topology of the excited PES along the reaction coordinates of apical or equatorial CO dissociation. Figure 4A reports the scans for the apical CO ligand release. As compared to the ground state,[28] the lower energy surfaces are loosely bound along the CO dissociation coordinate. Two series of surface crossings are observed (red arrows), the most evident starting from 5ex, and indicate putative dissociation pathways. The result of the calculation regarding the release of the equatorial CO ligand is shown in Supplementary Figure 13. The energy barrier for the CO dissociation (estimated from the difference between the excitation energies computed at the beginning and at the end of the PES scan, and averaged over the first 20 excited states) is twice as large for equatorial CO than for apical CO. Moreover, as described below, the dissociation of the apical CO along the pathway starting from 5ex appears almost barrierless.

We investigated the decay of the MLLCT 5ex state by optimizing its structure, taking the ground-state geometry as starting point, and then examining the geometry changes that result from each surface crossing (Figure 4B). The apical Fe−C bond is 0.04 Å longer in optimized 5ex than in the structure of the ground state, and the Fe−C−O angle bends 4.7°, which supports the dissociative nature of this excitation. This conclusion was further confirmed by TDDFT geometry optimization of the corresponding MLLCT state (12ex) of the Fe_2S_2 model in which side chain residues have been included (Supporting Information section 2.7). After optimization, 5ex can be considered a 5ex−4ex conical intersection, being only 0.06 kcal/mol higher than 4ex. Following the pathway depicted as an arrow in Figure 4A, we mimic the vibrational relaxation by a small stretch (+0.086 Å) of the apical Fe−C to force the crossing, reaching directly the 2ex state. After optimization, the 2ex structure is characterized by a significant lengthening and bending of the apical Fe−CO bond (+0.183 Å, 25.6°) as compared to the ground state. In a similar manner, we observed the decay of 2ex to 1ex, where, after optimization, the apical Fe−CO is partially dissociated. The 1ex surface crosses the ground state at d(Fe−C) = 2.523 Å (Supporting Information section 2.7). At this point, a small amount of vibrational energy should be sufficient to fully dissociate the Fe−C bond.

DOI: 10.1021/jacs.6b06603
J. Am. Chem. Soc. 2016, 138, 13612−13618

The results of the TDDFT investigation of the large Fe_6S_6 model (Figure 1C) show that the 5ex in the Fe_2S_2 model investigated above corresponds to a high energy excited state (242ex) in the large model (Supplementary Table 8 and Supplementary Figure 12a), consistent with the low energy excitations of the H-cluster being ineffective for CO release. We could not use the large Fe_6S_6 model (Figure 1C) to investigate the $Fe_4S_4 \rightarrow Fe_2S_2$ CT states because most of our attempts to use the spin-flip approach to optimize the geometry of the broken-symmetry $Fe_4S_4^{+}$−$Fe_2S_2^{-}$ species failed. However, we were able to optimize the structure of the 1ex Fe_6S_6 excited state, converging to a final structure in which the Fe−S bond that connects the cubane to the Fe_2S_2 subcluster is 0.13 Å longer than in the ground state, while all other distances are the same. This is consistent with the above qualitative argument according to which the CT states are not involved in CO dissociation.

DISCUSSION

We have defined the kinetics of the reaction with CO of the oxidized H-cluster of three distinct FeFe hydrogenases as a function of wavelength in the visible range and light power. The effects are about the same for the three enzymes that we studied despite differences in cofactor compositions: the enzyme from *Chlamydomonas reinhardtii* bears only the H-cluster, whereas the other two have additional electron transferring clusters.[1,23,34,35] Therefore, our experiments reveal an intrinsic property of the conserved H-cluster. From the point of view of the modeling, this implies that one only needs to investigate the photochemical properties of the H-cluster.

We have characterized before the "dark" kinetics of CO binding to and release from FeFe hydrogenases.[29,30,42] We have shown that the reaction can be described in terms of intramolecular diffusion of CO (leading to the reversible formation a "geminate state" with rate constants k_1 and k_{-1}), and reversible Fe_d−CO bond formation (rate constants k_2 and k_{-2}). We used the results of MD and DFT calculations to calculate all four individual rate constants, which we could combine to calculate the value of the rate of inhibition, which compares well with the experimental value.[42] Regarding the effect of light, the usual method for studying the photodissociation of CO from inorganic active sites consists of triggering CO release by a short laser pulse, and following the dissociation and rebinding using time-resolved spectroscopic techniques. Such investigation has only recently been carried out with a FeFe hydrogenase.[43] In the experiments presented in this Article, in contrast, we measure the steady-state effect of constant monochromatic illumination; the total concentration of enzyme−CO complex is not constant, but continuous irradiation nonetheless leads to a steady-state ratio of [E*−CO] over [E−CO] (Figure 5), which is determined by the competition between excitation, dissociative ($k_{-2}^{h\nu}$), and nondissociative ($k^{-h\nu}$) decay. Measuring the global rate of CO release informs on the nature and reactivity of the excited state that is formed upon illumination at a certain wavelength.

The simple binding/release kinetic model that we have used to analyze experiments carried out in the dark[29,30,42] can be fitted to the data recorded with the light on, showing that E*CO is in a quasi-steady state. We show in Supporting Information section 4 that the measured values of k_{in} and k_{out} are therefore related to the rate constants in Figure 5 by the following relations:

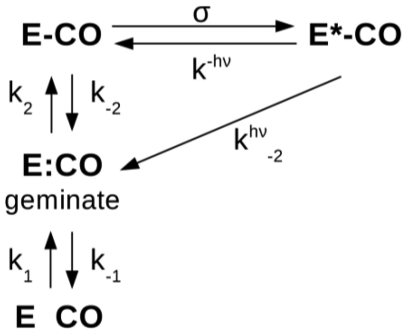

Figure 5. Kinetic scheme depicting the various steps that contribute to CO binding and (photo)release. Step "1" is the formation of a geminate state, from which the Fe−CO bond can be reversibly formed. The excited states decay either dissociatively or non-dissociatively.

$$k_{in} = k_1 k_2/(k_{-1} + k_2)$$

$$k_{out} = k_{-1}(k_{-2} + k_{-2}^{h\nu}\Lambda)/((1 + \Lambda)(k_{-1} + k_2))$$

where Λ is $\sigma I/(k^{-h\nu} + k_{-2}^{h\nu})$, with I the incident flux of photons, σ the cross section for light absorption, $k^{-h\nu}$ the rate at which the excited states decay without CO dissociation, and $k_{-2}^{h\nu}$ the rate at which the excited state dissociates CO. Our observation that the plot of k_{out} against P is a line (Figure 2D) shows that $\Lambda \ll 1$, consistent with the low absorption of the H-cluster. We conclude that at the low illumination power that we used, the excited states are populated more slowly than they decay either dissociatively or nondissociatively.

The absorption coefficient of H_{ox}−CO has not been published, but using the spectra of FeFe biomimetic complexes, we estimate $\varepsilon \approx 1$ mM^{-1} cm^{-1} in the 400 nm region.[9,44,45] Using $\sigma = \varepsilon \times \ln(10)/N_a$, the value of ε translates into a molecular absorption cross-section of 4.10^{-22} m^2 (for all transitions, dissociative and nondissociative). This value is very close to the cross section for the dissociative absorption of photons, 9.10^{-21} m^2 in Figure 2, suggesting that, at low wavelengths, most of the absorbed photons lead to photodissociation of the apical CO (thus $k^{-h\nu} \ll k_{-2}^{h\nu}$).

Thinking of the H-cluster in terms of a Fe_4S_4−Fe_2S_2 dyad system, a very common model in photochemistry, allowed us to predict which excitations are actually effective for CO release and to identify the relevant excitations in each photochemical process. This description emerges from the analysis of the H-cluster molecular orbitals in a natural manner and will probably prove useful in further investigations of its photochemical reactivity.

The most relevant point in this TDDFT investigation is the reliable correlation between the wavelengths that prove effective in the experiments and the computed excitation energies. We cannot expect TDDFT calculations to quantitatively predict the experimental excitations energies for such a negatively charged large system, but this level of theory is able to reproduce the features of the experimental absorption spectra available in the literature.[41]

Our calculations clearly show that only the excitations that involve the dinuclear subcluster are active with respect to CO photodissociation, and these are found at higher energy than the CT states. This conclusion qualitatively agrees with the experimental observation of ours that only irradiation in the high energy part of the visible spectrum increases the rate of CO dissociation.

DOI: 10.1021/jacs.6b06603
J. Am. Chem. Soc. 2016, 138, 13612−13618

Our PES analysis clearly indicates that dissociation of the apical CO is easier than that of the equatorial or bridging CO. This is not the consequence of the constraints provided by the protein. In the case of the first Fe_2S_2 localized state (5ex in the binuclear model), we could characterize in detail the pathway to the ground state, which is the barrierless release of the apical CO. In support of this result, we observed that if we include first-shell residue side chains in the calculation, the excited state that is equivalent to 5ex also shows barrierless apical CO dissociation (SI section 2.7 and Supplementary Figure 17). These theoretical results are fully consistent with our experimental observation that most violet/blue absorbed photons induce CO release (Figure 3).

It has been observed that visible irradiation at very low temperature (<8 K) also dissociates the apical CO from H_{ox}–CO, but distinct photoproducts (the structures of which were not fully clarified) are formed under certain cryogenic conditions, such as temperature in the range 15–30 K.[12−15] A possible explanation is that in this intermediate range of T, the greater vibrational energy of the system overcomes the barrier for the formation of a second photoproduct, which is not stable at room temperature and isomerizes to the most stable form.

Albracht and co-workers[14,15] have shown that white light damages the enzyme from *D. desulfuricans*, and suggested that this could be a result of the photolysis of one or more intrinsic CO ligands. We have observed no effect of light (in the wavelength and power ranges described here) on the turnover rate, which suggests that photodamage might be induced by higher energy and/or longer irradiation. We are now investigating, both theoretically and experimentally, the hypothesis that the UV irradiation might irreversibly inactivate the enzyme by inducing the release of intrinsic CO ligands or breaking of other Fe–ligand bonds.

TDDFT calculations being particularly challenging, it will be essential that further results be supported by experimental data. For example, one may oppose to the calculations presented here that TDDFT cannot describe excited states of double-excitation character, but our experiments actually rule out the relevance of double absorption. Indeed, we observe a linear dependence of the rate of dissociation on light power. Moreover, the absorption of the H-cluster is very weak (light absorption limits the rate of photorelease), making double-excitation very unlikely.

A limitation of our work is the low quality of the excitation energies that are calculated using pure GGA functionals such as BP86 and/or small models of the H-cluster, but our aim was not to reproduce the experimental spectrum; instead, it was to shed light on the first instants of the photodynamics of CO-inhibited H-cluster upon irradiation. Here, it is more important to describe the nature of the excitations than to accurately calculate their energies.

We believe that in the future, the elucidation of the photochemical processes will also help in understanding the reactivity of the active site in the dark, because the main electronic transitions involved in the excited states may occur as transient ground states either in the catalytic cycle or upon formation of inactive states under oxidative or reductive conditions.[17,46]

METHODS

Enzymes. We produced the FeFe hydrogenases from *C. acetobutilicum* and *C. reinhardtii* FeFe hydrogenases as described in ref 17. The enzyme from *M. elsdenii* was heterologously expressed in *E. coli* and activated as described in ref 47.

Electrochemistry. We covalently attached the enzymes onto pyrolytic edge graphite rotating electrodes (diameter 1 mm) using the method described in ref 31. We analyzed the electrochemical data using the model in ref 28 and the open source program available at www.qsoas.org.[48] We used laser components Flexpoint dot lasers, λ = 405 nm, 9.5 μW; λ = 450 nm, 11.1 μW ; λ = 532 nm, 11.3 μW; or λ = 635 nm, 8.1 μW. The diameter of the parallel beam was 5 mm. The power output could be tuned between 0 and 100% and measured with a Newton optical power meter 1916-C.

Computational Details. The quantum mechanics calculations performed have been carried out with the TURBOMOLE 7 suite of programs.[49] In particular, DFT and TDDFT calculations were carried out using the BP86 functional and an all-electron valence triple-ζ (def-TZVP) basis set with polarization functions on all atoms, in conjunction with the resolution-of-the-identity (RI) technique (Supporting Information section 1). Such computational approach proved appropriate for the correct representation of the electronic properties of the H-cluster, both considering binuclear Fe_2S_2 and complete Fe_6S_6 models, as reported in previous works.[3,28,38,50,51] The broken symmetry approach was implemented to reproduce the proper spin state of the full H-cluster model.[36,38,52]

ASSOCIATED CONTENT

Supporting Information

The Supporting Information is available free of charge on the ACS Publications website at DOI: 10.1021/jacs.6b06603.

DFT and TDDFT computational details and models; electronic structures of the models, CO-dissociation computed free energy barriers, TDDFT spectra of Fe_2S_2, Fe_2S_2 with residues, and Fe_6S_6 models (BP86 and/or PBE0), PES scans for the apical and equatorial CO dissociation, and explanation of the method used to study the CO dissociation pathway from 5ex; experimental PFV data for the CO-photodissociation for the FeFe hydrogenase of *C. reinhardtii* and *C. acetobutylicum*; experimental determination of the CO-release activation energy; and kinetic scheme and derivation of the rate constants used in the main text (PDF)

AUTHOR INFORMATION

Corresponding Authors

*leger@imm.cnrs.fr

*luca.bertini@unimib.it

Notes

The authors declare no competing financial interest.

ACKNOWLEDGMENTS

The French teams were supported by CNRS, Aix Marseille Université, INSA, CEA, Agence Nationale de la Recherche (ANR-12-BS08-0014, ANR-14-CE05-0010, LABEX program ARCANE ANR-11-LABX-0003-01), and the A*MIDEX grant (ANR-11-IDEX-0001-02) funded by the French Government "Investissements d'Avenir" program.

REFERENCES

(1) Fontecilla-camps, J. C.; Volbeda, A.; Cavazza, C.; Nicolet, Y. *Chem. Rev.* **2007**, *107*, 4273–4303.

(2) Lubitz, W.; Ogata, H.; Ru, O.; Reijerse, E. *Chem. Rev.* **2014**, *114*, 4081–4148.

(3) Greco, C.; Fourmond, V.; Baffert, C.; Wang, P.; Dementin, S.; Bertrand, P.; Bruschi, M.; Blumberger, J.; De Gioia, L.; Léger, C. *Energy Environ. Sci.* **2014**, *7* (11), 3543–3573.

DOI: 10.1021/jacs.6b06603
J. Am. Chem. Soc. 2016, 138, 13612–13618

(4) Thauer, R. K.; Käufer, B.; Zähringer, M.; Jungermann, K. *Eur. J. Biochem.* **1974**, *42* (2), 447−452.
(5) Pandelia, M. E.; Ogata, H.; Currell, L. J.; Flores, M.; Lubitz, W. *Biochim. Biophys. Acta, Bioenerg.* **2010**, *1797* (2), 304−313.
(6) Nicolet, Y.; Lacey, A. L.; De Vernede, X.; Fernandez, V. M.; Hatchikian, E. C.; Fontecilla-camps, J. C. *J. Am. Chem. Soc.* **2001**, *123*, 1596−1601.
(7) Fan, H.; Hall, M. B. *J. Am. Chem. Soc.* **2001**, *123*, 3828−3829.
(8) Silakov, A.; Wenk, B.; Reijerse, E.; Lubitz, W. *Phys. Chem. Chem. Phys.* **2009**, *11*, 6592−6599.
(9) Berggren, G.; Adamska, A.; Lambertz, C.; Simmons, T. R.; Esselborn, J.; Atta, M.; Gambarelli, S.; Mouesca, J.-M.; Reijerse, E. J.; Lubitz, W.; Happe, T.; Artero, V.; Fontecave, M. *Nature* **2013**, *499* (7456), 66−69.
(10) Lemon, B. J.; Peters, J. W. *J. Am. Chem. Soc.* **2000**, *122* (15), 3793−3794.
(11) Parkin, A.; Cavazza, C.; Fontecilla-Camps, J. C.; Armstrong, F. A. *J. Am. Chem. Soc.* **2006**, *128* (4), 16808−16815.
(12) Chen, Z.; Lemon, B. J.; Huang, S.; Swartz, D. J.; Peters, J. W.; Bagley, K. A. *Biochemistry* **2002**, *41*, 2036−2043.
(13) Silakov, A.; Reijerse, E. J.; Lubitz, W. *Eur. J. Inorg. Chem.* **2011**, *2011* (7), 1056−1066.
(14) Albracht, S. P. J.; Roseboom, W.; Hatchikian, E. C. *JBIC, J. Biol. Inorg. Chem.* **2006**, *11* (1), 88−101.
(15) Roseboom, W.; De Lacey, A. L.; Fernandez, V. M.; Hatchikian, E. C.; Albracht, S. P. J. *JBIC, J. Biol. Inorg. Chem.* **2006**, *11* (1), 102−118.
(16) Senger, M.; Mebs, S.; Duan, J.; Wittkamp, F.; Apfel, U.-P.; Heberle, J.; Haumann, M.; Stripp, S. T. *Proc. Natl. Acad. Sci. U. S. A.* **2016**, *113* (30), 8454−8459.
(17) Fourmond, V.; Greco, C.; Sybirna, K.; Baffert, C.; Wang, P.; Ezanno, P.; Montefiori, M.; Bruschi, M.; Meynial-Salles, I.; Soucaille, P.; Blumberger, J.; Bottin, H.; De Gioia, L.; Léger, C. *Nat. Chem.* **2014**, *6* (4), 336−342.
(18) Gust, D.; Moore, T. A.; Moore, A. L. *Acc. Chem. Res.* **2009**, *42* (12), 1890−1898.
(19) Lubner, C. E.; Applegate, A. M.; Knörzer, P.; Ganago, A.; Bryant, D. A.; Happe, T.; Golbeck, J. H. *Proc. Natl. Acad. Sci. U. S. A.* **2011**, *108* (52), 20988−20991.
(20) Ghirardi, M. L. *Photosynth. Res.* **2015**, *125* (3), 383−393.
(21) Lee, C.; Park, H. S.; Fontecilla-camps, J. C.; Reisner, E. *Angew. Chem., Int. Ed.* **2016**, *55*, 5971−5974.
(22) Ciaccafava, A.; Hamon, C.; Infossi, P.; Marchi, V.; Giudici-Orticoni, M.-T.; Lojou, E. *Phys. Chem. Chem. Phys.* **2013**, *15* (39), 16463−16467.
(23) Peters, J. W.; Lanzilotta, W. N.; Lemon, B. J.; Seefeldt, L. C. *Science* **1998**, *282* (5395), 1853−1858.
(24) Li, Y.; Rauchfuss, T. B. *Chem. Rev.* **2016**, *116* (12), 7043−7077.
(25) Kania, R.; Frederix, P. W. J. M.; Wright, J. a; Ulijn, R. V.; Pickett, C. J.; Hunt, N. T. *J. Chem. Phys.* **2012**, *136* (4), 44521.
(26) Caplins, B. W.; Lomont, J. P.; Nguyen, S. C.; Harris, C. B. *J. Phys. Chem. A* **2014**, *118* (49), 11529−11540.
(27) Bertini, L.; Greco, C.; Fantucci, P.; De Gioia, L. *Int. J. Quantum Chem.* **2014**, *114* (13), 851−861.
(28) Bertini, L.; Fantucci, P.; De Gioia, L.; Zampella, G. *Inorg. Chem.* **2013**, *52*, 9826−9841.
(29) Liebgott, P.; Leroux, F.; Burlat, B.; Dementin, S.; Baffert, C.; Lautier, T.; Fourmond, V.; Ceccaldi, P.; Cavazza, C.; Meynial-Salles, I.; Soucaille, P.; Fontecilla-Camps, J. C.; Guigliarelli, B.; Bertrand, P.; Rousset, M.; Léger, C. *Nat. Chem. Biol.* **2010**, *6* (1), 63−70.
(30) Baffert, C.; Bertini, L.; Lautier, T.; Greco, C.; Sybirna, K.; Ezanno, P.; Etienne, E.; Soucaille, P.; Bertrand, P.; Meynial-salles, I.; De Gioia, L.; Léger, C. *J. Am. Chem. Soc.* **2011**, *133*, 2096−2099.
(31) Baffert, C.; Sybirna, K.; Ezanno, P.; Lautier, T.; Hajj, V.; Meynial-Salles, I.; Soucaille, P.; Bottin, H.; Léger, C. *Anal. Chem.* **2012**, *84* (18), 7999−8005.
(32) Léger, C.; Dementin, S.; Bertrand, P.; Rousset, M.; Guigliarelli, B. *J. Am. Chem. Soc.* **2004**, *126* (38), 12162−12172.
(33) Orain, C.; Saujet, L.; Gauquelin, C.; Soucaille, P.; Meynial-Salles, I.; Baffert, C.; Fourmond, V.; Bottin, H.; Léger, C. *J. Am. Chem. Soc.* **2015**, *137* (9), 12580−12587.
(34) Mulder, D. W.; Boyd, E. S.; Sarma, R.; Lange, R. K.; Endrizzi, J. a; Broderick, J. B.; Peters, J. W. *Nature* **2010**, *465* (7295), 248−251.
(35) Nicolet, Y.; Piras, C.; Legrand, P.; Hatchikian, C. E.; Fontecilla-Camps, J. C. *Structure* **1999**, *7* (1), 13−23.
(36) Fiedler, A. T.; Brunold, T. C. *Inorg. Chem.* **2005**, *44* (25), 9322−9334.
(37) Siegbahn, P. E. M.; Tye, J. W.; Hall, M. B. *Chem. Rev.* **2007**, *107*, 4414−4435.
(38) Bruschi, M.; Greco, C.; Bertini, L.; Fantucci, P.; Ryde, U.; De Gioia, L. *J. Am. Chem. Soc.* **2010**, *132*, 4992−4993.
(39) Bertini, L.; Greco, C.; Bruschi, M.; Fantucci, P.; De Gioia, L. *Organometallics* **2010**, *29* (9), 2013−2025.
(40) Hunt, N. T.; Wright, J. A.; Pickett, C. *Inorg. Chem.* **2016**, *55* (2), 399−410.
(41) Swanson, K. D.; Ratzloff, M. W.; Mulder, D. W.; Artz, J. H.; Ghose, S.; Hoffman, A.; White, S.; Zadvornyy, O. A.; Broderick, J. B.; Bothner, B.; King, P. W.; Peters, J. W. *J. Am. Chem. Soc.* **2015**, *137* (5), 1809−1816.
(42) Kubas, A.; Orain, C.; De Sancho, D.; Saujet, L.; Sensi, M.; Gauquelin, C.; Meynial-Salles, I.; Soucaille, P.; Bottin, H.; Baffert, C.; Fourmond, V.; Best, R.; Blumberger, J.; Léger, C. *Nat. Chem.* **2016**, DOI: 10.1038/nchem.2592.
(43) Mirmohades, M.; Adamska-Venkatesh, A.; Sommer, C.; Reijerse, E.; Lomoth, R.; Lubitz, W.; Hammarström, L. *J. Phys. Chem. Lett.* **2016**, *7* (16), 3290−3293.
(44) Roy, S.; Jones, A. K. *Nat. Chem. Biol.* **2013**, *9* (10), 603−605.
(45) Thornley, W. A.; Bitterwolf, T. E. *Chem. - Eur. J.* **2015**, *21*, 18218−18229.
(46) Hajj, V.; Baffert, C.; Sybirna, K.; Meynial-Salles, I.; Soucaille, P.; Bottin, H.; Fourmond, V.; Léger, C. *Energy Environ. Sci.* **2014**, *7* (2), 715.
(47) Caserta, G.; Adamska-Venkatesh, A.; Pecqueur, L.; Atta, M.; Artero, V.; Souvik, R.; Reijerse, E.; Lubitz, W.; Fontecave, M. *Biochim. Biophys. Acta, Bioenerg.* **2016**, *1857* (11), 1734−1740.
(48) Fourmond, V. *Anal. Chem.* **2016**, *88*, 5050−5052.
(49) Ahlrichs, R.; Bär, M.; Häser, M.; Horn, H.; Kölmel, C. *Chem. Phys. Lett.* **1989**, *162* (3), 165−169.
(50) Stiebritz, M. T.; Reiher, M. *Inorg. Chem.* **2009**, *48* (15), 7127−7140.
(51) Liu, C.; Liu, T.; Hall, M. B. *J. Chem. Theory Comput.* **2015**, *11* (1), 205−214.
(52) Bruschi, M.; Greco, C.; Fantucci, P.; De Gioia, L. *Inorg. Chem.* **2008**, *47* (13), 6056−6071.

DOI: 10.1021/jacs.6b06603
J. Am. Chem. Soc. 2016, 138, 13612−13618